Chemical Papers (2024) 78:1647–1658
https://doi.org/10.1007/s11696-023-03192-6

ORIGINAL PAPER

Synthesis and characterization studies of facile $CuO:La_2O_3$ nanomaterial and its role as electrode for overall energy storage and energy generation applications

Sundus Azhar[1] · Khuram Shahzad Ahmad[1] · Isaac Abrahams[2] · Tenzin Ingsel[3] · Ram K. Gupta[3] · Adel El-marghany[4]

Received: 3 August 2023 / Accepted: 31 October 2023 / Published online: 5 December 2023

Abstract

The current study implements an environmental-friendly and sustainable methodology to fabricate $CuO:La_2O_3$-based electrode by using phyto-aqueous extract derived from the Amaranthus viridis plant leaves. $CuO:La_2O_3$ was synthesized in several concentrations ranging from 2.5 to 10%. The synthesized nanoparticles revealed varied morphology for different concentrations with a varying crystalline size in the range of 18.2–43.44 nm. The lowest optical band gap energy of 3.25 eV was observed for 7.5% doped concentration. Taking advantage of its unique morphology and lower crystalline size, 7.5% $CuO:La_2O_3$ was specifically selected to be utilized as an electrode material for subsequent investigations involving supercapacitor and water splitting studies. The supercapacitor behavior was studied using cyclic voltammetry (CV) and galvanostatic charge discharge (GCD) techniques. The specific capacitance value of 879.6 F/g was obtained for the fabricated electrode. The water splitting studies revealed the better potential of fabricated electrocatalyst for oxygen evolution reaction with an overpotential value of 351 mV as compared to that of hydrogen evolution reaction where the overpotential value of 182 mV was observed. Moreover, the fabricated electrocatalyst showed excellent cyclic stability for more than 2000 cycles and up to 20 h. Nevertheless, comprehensive findings displayed $CuO:La_2O_3$ as an efficient energy storage material as well as promising catalytic material for the water splitting studies.

Graphical abstract

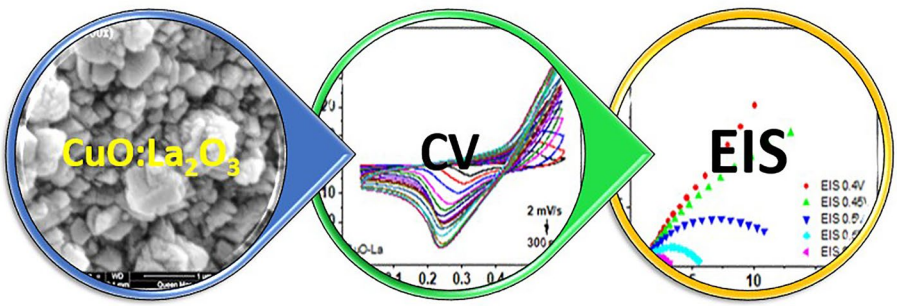

Keywords Nanomaterials · CuO · Lanthanum oxide · Supercapacitor · Water splitting

Introduction

The global energy crisis is escalating because of population growth, and one of the major concerns of present times is to cater the energy needs of this growing population. The current energy predicament is leading to increased depletion of fossil fuel reserves which have a detrimental effect on the environment (Nandi et al. 2020; Veerakumar et al. 2020). This reliance on the fossil-based fuels has severe implications, as they adversely affect earth biota from emission of hazardous and poisonous pollutants (Huang and Lin 2018; Yumak et al. 2019). Therefore, to ensure and

Extended author information available on the last page of the article

promote sustainable environment, scientists and engineers are actively involved in the research and development of alternate, more affordable, clean and green renewable energy solutions. This includes exploring options such as solar energy, hydrogen energy, wind energy and more. Another task is the efficient storage of the generated energy, and in order to fully commercialize these renewable energy generating systems, efficient energy storage capacities are crucial. In the recent times, production of energy through water splitting process and supercapacitors in terms of energy storage devices have emerged as a most popular electrochemical application (Huang and Lin 2018; Yumak et al. 2019). However, efficiency of these electrochemical applications greatly depends on the electrode material used, and currently, there has been specific focus on fabrication of efficient as well as cost-effective electrode material for supercapacitor and water splitting applications (Wei et al. 2018; Zequine et al. 2019).

The employment of "MO x"-based nanomaterials as electrodes embraces immense potential due to their promising characteristics, including competent and shorter diffusion pathways, as well as increased active sites for rapid ion or electron transport. These features also contribute to lower internal resistance and enhanced electrochemical conductivity (Yan et al. 2019; Tomboc et al. 2021; Dinesh et al., 2020; Chen et al. 2020). There are various methods to synthesize nanoparticles including chemical, physical as well as biological route; however, the synthesis of novel metal oxide-based nanomaterials with minimal agglomeration is a significant challenge for researchers. The complexity associate with physical synthesis routes and the use of toxic chemicals in chemical synthesis route are the reasons that scientists are finding biological synthesis route more convenient in terms of environmental sustainability as well as economically as this method use organic entities of microbes and plants as a reducing and the capping agents for the synthesis of nanoparticles (Wang et al. 2019; Wei et al. 2018).

In the present study, we adopted green and clean biological synthesis route using leaves of Amaranthus viridis L. (AVL) plant for synthesis of lanthanum-doped copper oxide nanomaterials and used these nanoparticles to fabricate the electrode materials to study its potential for energy generation and storage applications. AVL plant is a medicinal plant possessing huge phytochemicals which could act as the reducing-cum-capping agents in synthesis of nanoparticles. CuO nanomaterials are reported as potential electrode materials for energy generation and storage because of their properties such as narrow band gap, non-toxicity and low cost which makes it suitable material for the various electrochemical as well as photovoltaic applications. However, CuO is barely reported as a single agent for supercapacitor applications due to its lower specific capacitance. Therefore, to enhance efficiency, the scientists are investigating other CuO-based materials (Shinde et al. 2019; Kumar et al. 2021; Zhang et al. 2020). Mariadhas et al., 2023 reported synthesis of novel Ag-CuO@GO nanocomposites using tea plant extract as reducing and capping agent for photocatalytic applications (Mariadhas et al. 2023). Raveesha et al., 2019 successfully synthesized magnesium- and iron-doped CuO nanoparticles using leaf extract of the *Costus pictus* plant for electrochemical and antibacterial analysis (Raveesha et al. 2019). In our previous work, we have successfully synthesized CuO/BiO nanocomposite using AVL plant leaves and studied its potential for HER and OER as well as for energy storing devices as an electrode (Azhar et al., 2021). The promising results from previous study encouraged us to explore more CuO-based nanomaterials. Accordingly, in the current study we are reporting synthesis of doped CuO:La_2O_3 nanomaterial in different concentrations using AVL foliar extract. The different doped concentrations of synthesized nanomaterial were characterized thoroughly using the UV–Vis, FT-IR, XRD, SEM and EDX, and then, the concentration with most favorable and promising results was explored further as a supercapacitor electrode material and as catalyst for water splitting applications.

Material and methods

Copper (II) acetate monohydrate, $Cu(CH_3COO)$ (with purity of ≥ 97.5%), and lanthanum (III) acetate hydrate, $C_6H_9LaO_6{\cdot}xH_2O$ (with a purity of 96%), were acquired from Sigma-Aldrich, Germany. Deionized (DI) water was used throughout the experiments. The aqueous leaf extract of Amaranthus viridis L. (AVL) served as the reducing and capping agent. For the fabrication of electrode material, *N*-methyl pyrrolidinone and polyvinylidene difluoride (PVDF) were obtained from Strem chemicals and Alfa Aesar, respectively. Analytical-grade ethanol (C_2H_5OH), with a purity of 99%, acetylene black and potassium hydroxide (KOH) were attained from VWR Chemicals BDH.

Synthesis of CuO:La_2O_3 nanomaterial

In our previous study, we have reported a detail account on the preparation of AVL aqueous leaf extract.[18] In the current research, a measured amount of 0.3993 g of copper (II) acetate monohydrate was mixed in 100 mL of deionized water to make a precursor solution of 20 mM named as solution A. Additionally, another 20 mM solution of lanthanum acetate hydrate was synthesized by dissolving 0.6321 g of lanthanum acetate hydrate in 100 mL of deionized water referred to as solution B. Both solutions were mixed separately using magnetic stirring for 20 to 30 min without any heat treatment. Four different doping concentrations ranging from 2.5 to 10% were prepared using solution A and solution

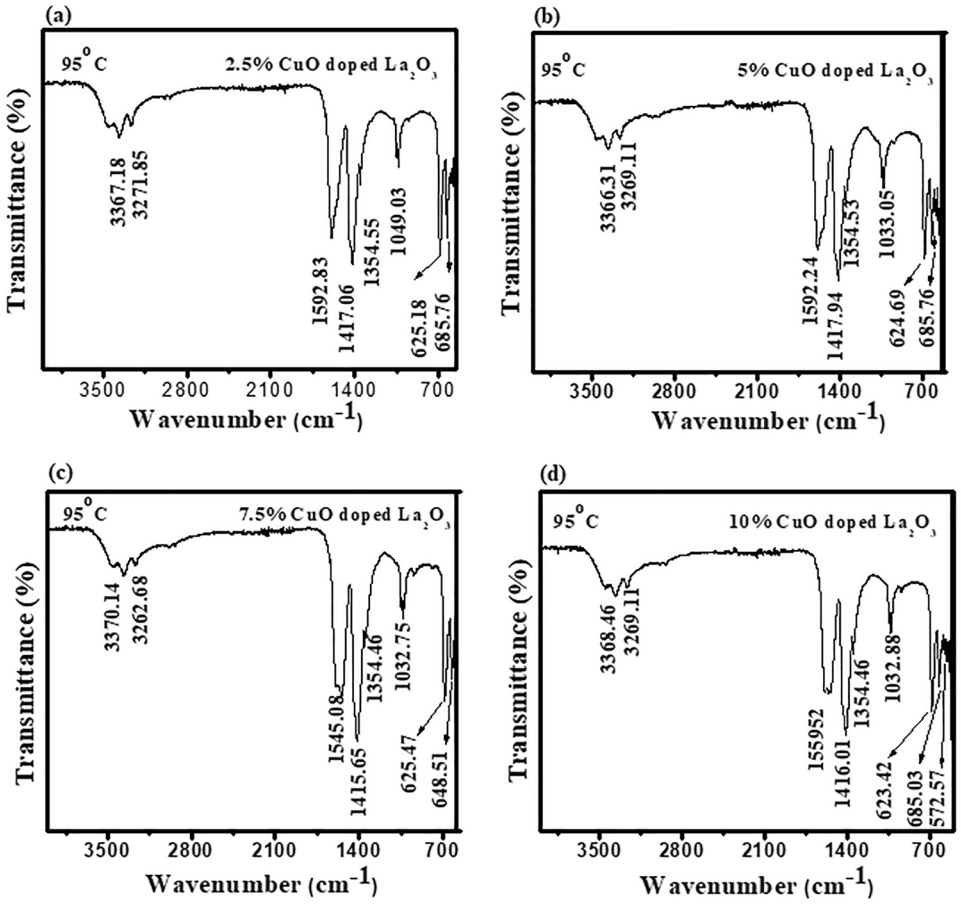

Fig. 1 FTIR analysis of copper oxide doped by lanthanum oxide in various concentrations before calcination: **a** 2.5% CuO:La_2O_3, **b** 5% CuO:La_2O_3, **c** 7.5% CuO:La_2O_3, **d** 10% CuO:La_2O_3

B. 10 mL of the organized AVL extract was added to each precursor solution while stirring at 70 °C. All synthesized concentrations underwent magnetic stirring for approximate 2 h at 70 °C followed by overnight storage in dark conditions under room temperature. The aged solutions were then evaporated using oven at 96 °C to obtain dried powder samples. These dried samples were then subsequently calcined at high temperature of 450 °C for time duration of 4 h to obtain doped concentrations of 2.5, 5, 7.5 and 10% La_2O_3-doped CuO (abbreviated as 2.5% CuO:La_2O_3, 5% CuO:La_2O_3, 7.5% CuO:La_2O_3 and 10% CuO:La_2O_3, respectively).

Characterization techniques

All synthesized CuO:La_2O_3 nanomaterials underwent various characterization techniques including FTIR (i.e., PerkinElmer Spectrum 10/65 FTIR spectrometer), UV–Vis spectroscopy (i.e., Agilent Cary 100 UV–Vis spectrometer) and X-ray powder diffraction (i.e., PANalytical Cubi X3 XRD instrument). Additionally, elemental analysis using energy-dispersive spectroscopy (EDX) and field emission imaging by scanning electron microscope (FE*SEM*) was performed by "FEI Quanta 3d ESEM" instruments.

Electrode fabrication

The preparation of working electrode material (7.5% CuO:$La_2O_{3)}$ was assisted by AVL facilitation. The 80% by weight of prepared nanomaterial was mixed by amalgamation with acetylene black (10%) by weight. Additionally, 10% by weight of PVDF was also included along with N-methyl pyrrolidinone (NMP). The resulting mixture was mixed well and then deposited on the Ni foam substrate. Subsequently the electrode underwent a drying process inside the oven at temperature of 60 °C for time duration of 12 h. The fabricated electrode was then subjected to analysis by focusing its promising features for OER/HER and supercapacitance.

Electrochemical characterization

To carry out the electrochemical characterization, a widely used workstation of Princeton Applied Research (USA) equipped with a standard conventional electrode configuration was utilized. The electrochemical experiments were functioned in three working electrode system using a specifically prepared Ni foam as working electrode, the counter electrode consisted of platinum wire and a "SCE" electrode

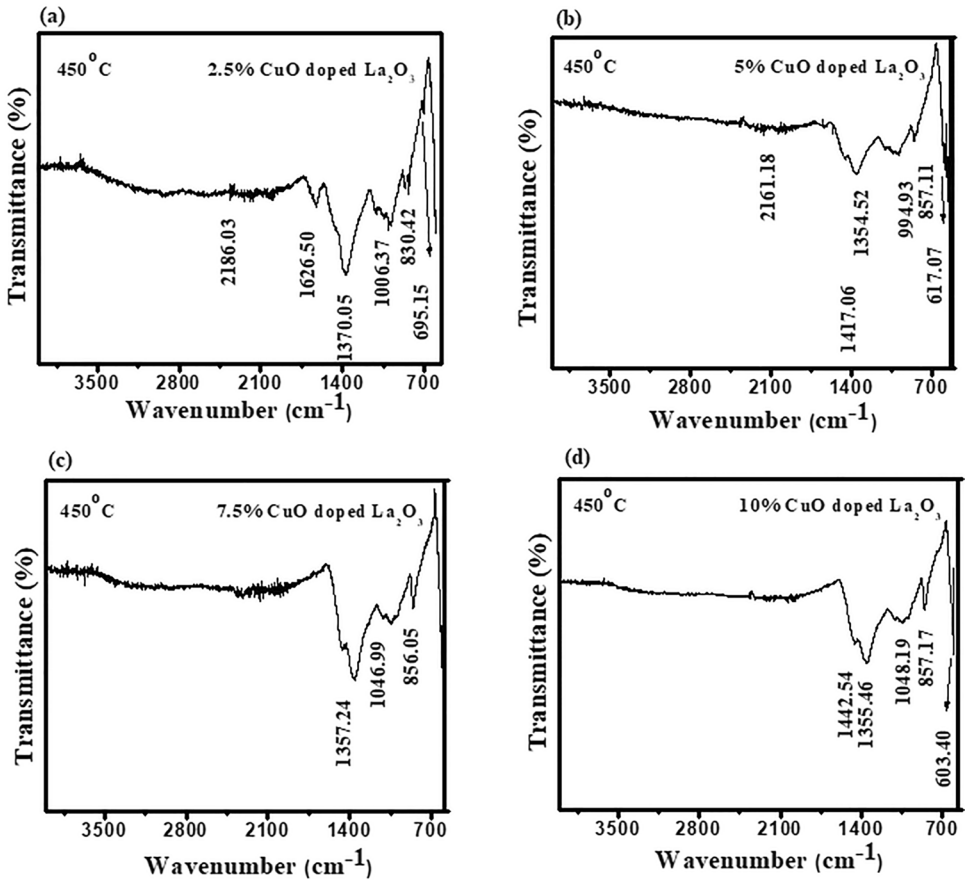

Fig. 2 After calcination FTIR analysis of lanthanum-doped copper oxide in various concentrations: **a** 2.5% CuO:La_2O_3, **b** 5% CuO:La_2O_3, **c** 7.5% CuO:La_2O_3, **d** 10% CuO:La_2O_3

which is a saturated calomel electrode (SCE) as reference. Various electrochemical techniques were utilized, encompassing cyclic voltammetry (CV), galvanostatic charge–discharge (GCD), linear sweep voltammetry (LSV) and electrochemical impedance spectroscopy (EIS) among other methods.

Result and discussion

The AVL aqueous extract exhibits significant amount of phytochemicals (as given in supplementary file); thus, it was used to synthesize CuO:La_2O_3 nanomaterials. CuO was doped by La_2O_3 in concentration ranged from 2.5 to 10% and analyzed by FTIR before and after calcination to study role of the organic functional groups of AVL plant in synthesis of the doped CuO nanoparticles.

Figure 1 reveals the FTIR analysis for all doped concentrations of oven-dried nanomaterials. The FTIR vibrational peaks of La_2O_3-doped CuO in between 4000 and 500 cm^{-1} can be seen in all images of Fig. 1a–d. Notable peak frequencies in the range of 1600–500 cm^{-1} were detected. These peak vibrations are indicating the alkynes, alkanes, carboxylic acid, aromatics and metal oxide bonds (Shaheen et al. 2020; Zahra et al. 2020). The occurrences of alkynes, alkanes, carboxylic acid, as well as aromatics are indicating the stabilizing and capping agents of AVL.

Figure 2a–d indicates the vibrational peaks of FTIR for all four doped concentrations after calcination of nanoparticles at 450°C. Many peaks observed at 95°C have disappeared in Fig. 2a–d. This can be due to high temperature treatment which caused complete removal of some of the phyto-groups and degraded others into their metabolites which resulted in emergence of new peaks. However, alkynes (–C=C– stretch) and alkanes (C–H) observed in Fig. 2 are indicating phyto-metabolites of the Amaranthus *viridis* plant extract which played significant role in the stabilization of synthesized nanomaterial.

The X-ray diffraction patterns/peaks of La_2O_3-doped CuO are presented in Fig. 3. CuO phase was determined in agreement with 00-048-1548 ICSD file for 2.5% CuO:La_2O_3, 5% CuO:La_2O_3 and 7.5% CuO:La_2O_3, whereas peak patterns of 10% CuO:La_2O_3 were matched well with ICSD file 00-005-0667. However, La_2O_3 phase was revealed in consistency with 00-005-0602 ICSD file for 2.5% CuO:La_2O_3 and 7.5% CuO:La_2O_3, whereas ICSD file 00–022-0369 matched well with 5% CuO:La_2O_3 and 10% CuO:La_2O_3.

The crystal size of the different doped concentrations was calculated by using Debye–Scherrer equation (Eq. 1):

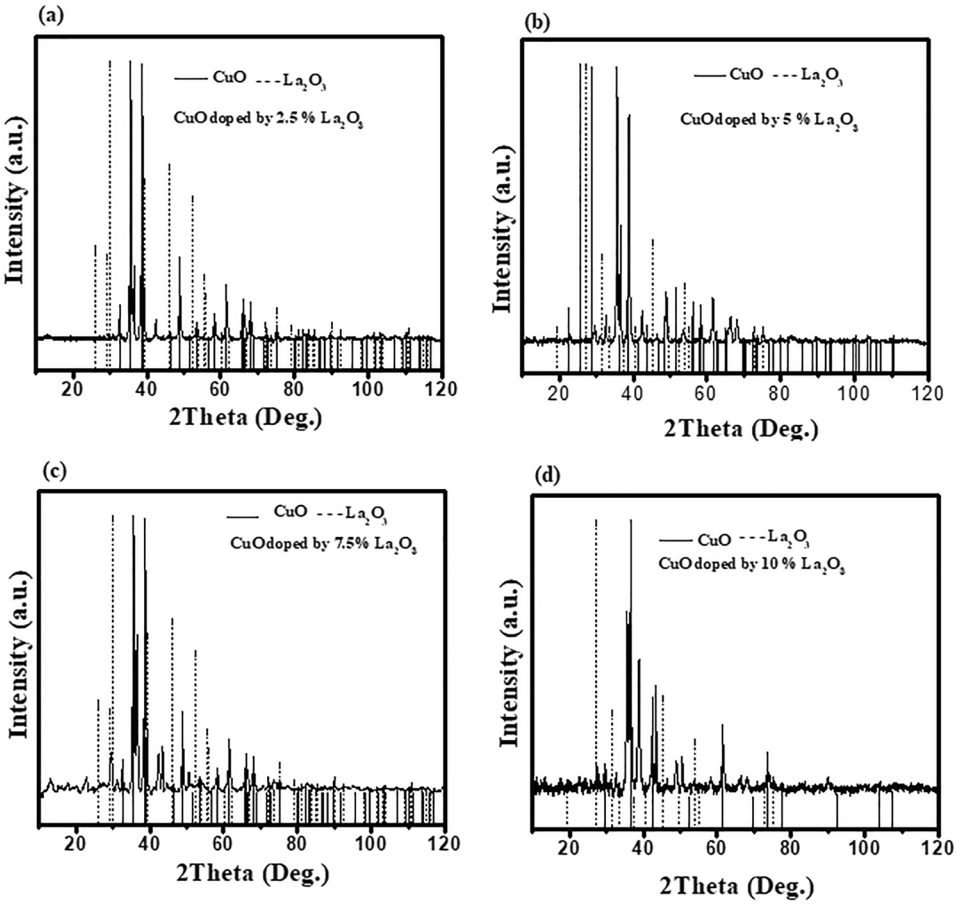

Fig. 3 XRD pattern of doped copper oxide in various concentrations: **a** 2.5% $CuO:La_2O_3$, **b** 5% $CuO:La_2O_3$, **c** 7.5% $CuO:La_2O_3$, **d** 10% $CuO:La_2O_3$

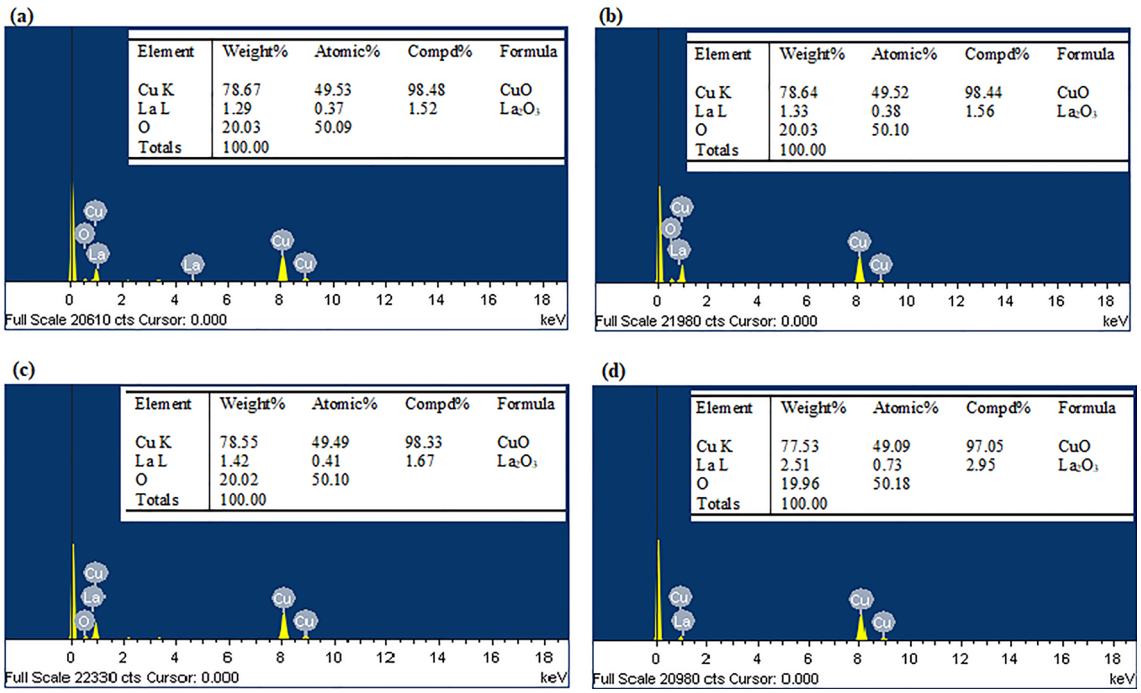

Fig. 4 EDX pattern of lanthanum-doped copper oxide in various concentrations: **a** 2.5% $CuO:La_2O_3$, **b** 5% $CuO:La_2O_3$, **c** 7.5% $CuO:La_2O_3$, **d** 10% $CuO:La_2O_3$

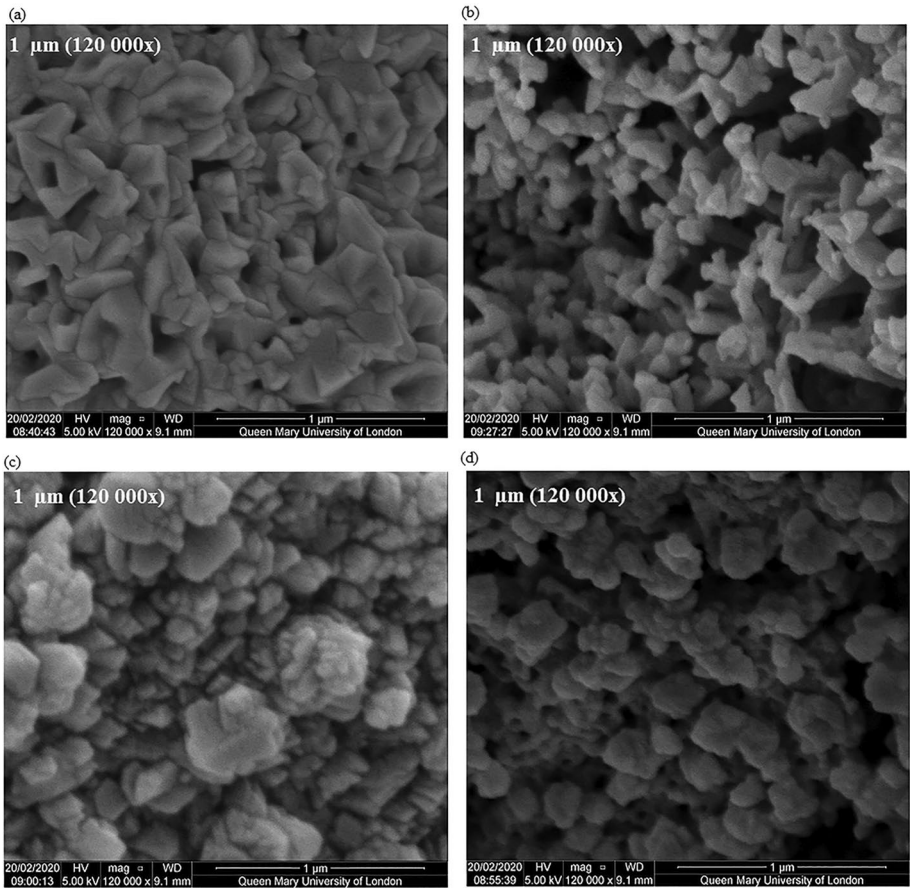

Fig. 5 FESEM images of lanthanum-doped copper oxide in various concentration at 1 µm: **a** 2.5% CuO:La_2O_3, **b** 5% CuO:La_2O_3, **c** 7.5% CuO:La_2O_3, **d** 10% CuO:La_2O_3

$$D = \left[\frac{K\lambda}{\beta \mathrm{Cos}\theta}\right] xA. \quad (1)$$

Here, D stands for the grain size, K refers to the Scherrer's constant, θ signifies the diffraction pattern, λ is wavelength and β corresponds to the full width at half maximum (FWHM). The crystallite size of 26.58, 29.32, 18.12 and 43.44 was observed for 2.5% La_2O_3-doped CuO, 5% La_2O_3-doped CuO, 7.5% La_2O_3-doped CuO and 10% La_2O_3-doped CuO, respectively. It is worth noticing that the maximum crystal size was observed for the doping concentration of 10% lanthanum-doped CuO while the crystal size of other La_2O_3-doped CuO materials showed the trend as given below:

% CuO:La_2O_3 < 2.5% CuO:La_2O_3 < 5% CuO:La_2O_3 < 10% CuO:La_2O_3.

Figure 4a–d presents EDX spectrum of La_2O_3-doped CuO at adopted concentrations. Cu, La and O were found in the elemental composition of the synthesized materials, whereas atomic percent and weight percent of La were observed to be increasing from 2.5 to 10% concentrations in Fig. 4a–d, respectively. Figure 4 shows 0.37% atomic percent of La for 2.5% CuO:La_2O_3 while in Fig. 4d, 10% CuO:La_2O_3 showed atomic percentage of 2.95%. Nevertheless, no elemental impurity was revealed in the EDX analysis for CuO:La_2O_3 nanomaterials.

Figure 5a–d depicts the morphology of AVL-assisted doped concentrations of CuO:La_2O_3 nanomaterials at 1 µm magnification. The cluster of particles are observed in Fig. 5a with wavelike surface, or this could be wavelike arrangements of particles. The spherical and irregular shaped particles were found for 5 CuO:La_2O_3 as shown in Fig. 5b while flowerlike structures are shown in Fig. 5c for 7.5% CuO:La_2O_3. Figure 5d of 10% CuO:La_2O_3 also exhibits spherical particles with more agglomeration. The agglomeration is generally associated with the particles of doped materials (Tian et al. 2015; Mersian et al. 2018) However, comparatively less agglomerated particles with the definitive shapes were observed for 7.5% CuO:La_2O_3 which could be well supported by lower crystal size determined by X-ray diffraction patterns.

The Tauc plots of CuO doped by La_2O_3 are presented in Fig. 6a–d with inset of UV absorbance spectrum. The band gap of doped concentrations of CuO:La_2O_3 nanoparticles was calculated through Tauc plot by using Eq. (2):

$$(\alpha hv)\, A1(hv\_Eg). \quad (2)$$

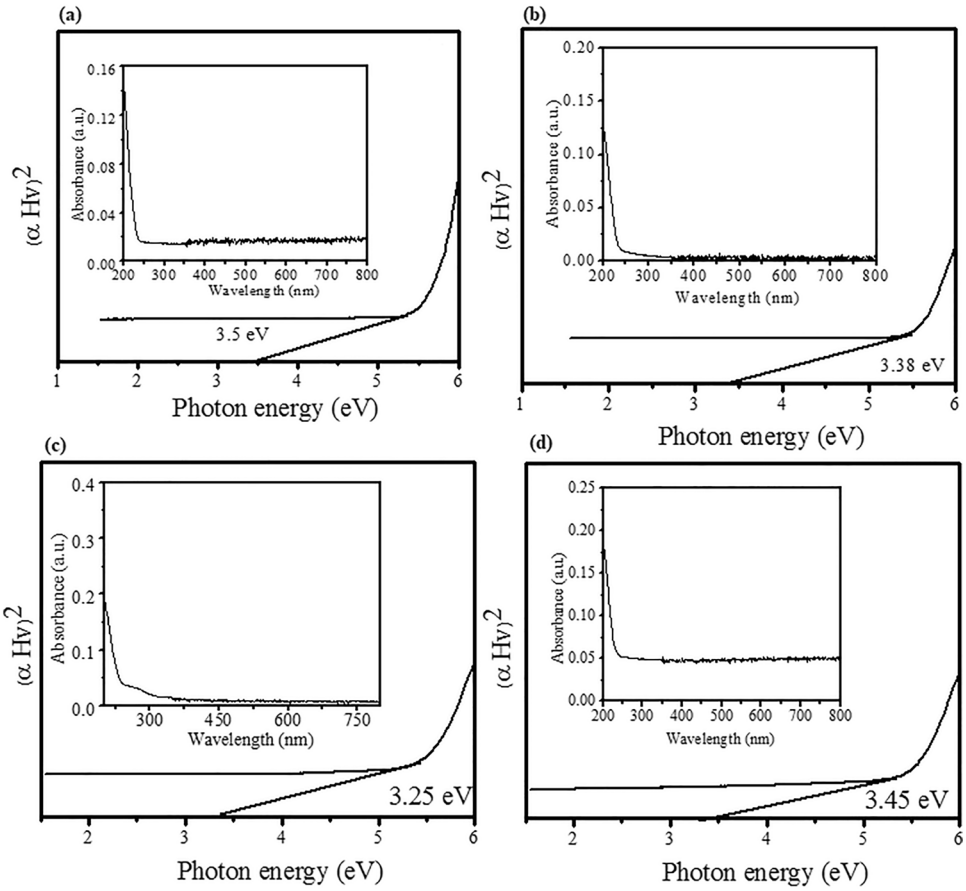

Fig. 6 Tauc plots of different lanthanum-doped copper oxide concentrations: **a** 2.5% CuO:La_2O_3, **b** 5% CuO:La_2O_3, **c** 7.5% CuO:La_2O_3, **d** 10% CuO:La_2O_3

Here α stands for the absorption coefficient, Eg represents the band gap energy and hv depicts photon. Figure 6a reveals the band gap of 3.5 eV for 2.5% CuO:La_2O_3, whereas with the increase of doping percentage up to 5% the band gap energy value of 3.38 eV was obtained as shown in Fig. 6b. The value of band gap was further reduced to 3.25 eV as shown in Fig. 6c for 7.5% CuO:La_2O_3 but higher band gap value of 3.45 eV was observed for the 10% doping concentration as shown in Fig. 6d. Consequently, the lowest band gap energy was observed for 7.5% CuO:La_2O_3 while overall band gap value ranged from 3.25 to 3.55 eV for CuO:La_2O_3 nanomaterials.

Supercapacitor and Water Splitting

In the current study, 7.5% CuO:La_2O_3 nanomaterial showed the lower crystal size and less agglomerated morphology as compared to other doping concentrations. These features are greatly favorable for the promising electrochemical behavior of the material. Hence, the AVL-assisted 7.5% CuO:La_2O_3-based electrode was fabricated for the further investigation of its potential in energy-based applications.

To determine the supercapacitive performance, the fabricated CuO:La_2O_3 electrode was explored by the cyclic voltammetry (CV) as well as galvanostatic charge discharge (GCD) techniques as shown in Fig. 6a–b. The cyclic voltammetric curves in Fig. 6a exhibiting the prominent redox peaks are indicative of Faradic reaction-based pseudocapacitors (Mersian et al. 2018; Sayyed et al. 2019; Veerakumar et al. 2020). Pseudocapacitors are the type of the capacitors which uses redox materials, e.g., metal oxides or conducting polymers and preserve energy by following the mechanism of Faradic reactions (Zheng et al. 2019; Ramesh et al. 2018). The redox reaction of CuO:La_2O_3-based electrode can be explained as follow (Dubal et al. 2013):

$$2CuO + 2H^+ + 2e^- \leftrightarrow Cu_2O\,(OH).$$

Furthermore, the behavior of the electrode and rate capability was analyzed by running CV scans at numerous scan rates from 2 to 300 mV/s. Figure 7a evidently shows that the shape of CV curves stayed stable throughout the scan rates. Corresponding to (Bhagwan et al. 2020; Shaheen et al. 2021), consistence of the CV shapes throughout the applied scan rates signifies the promising rate capability of the

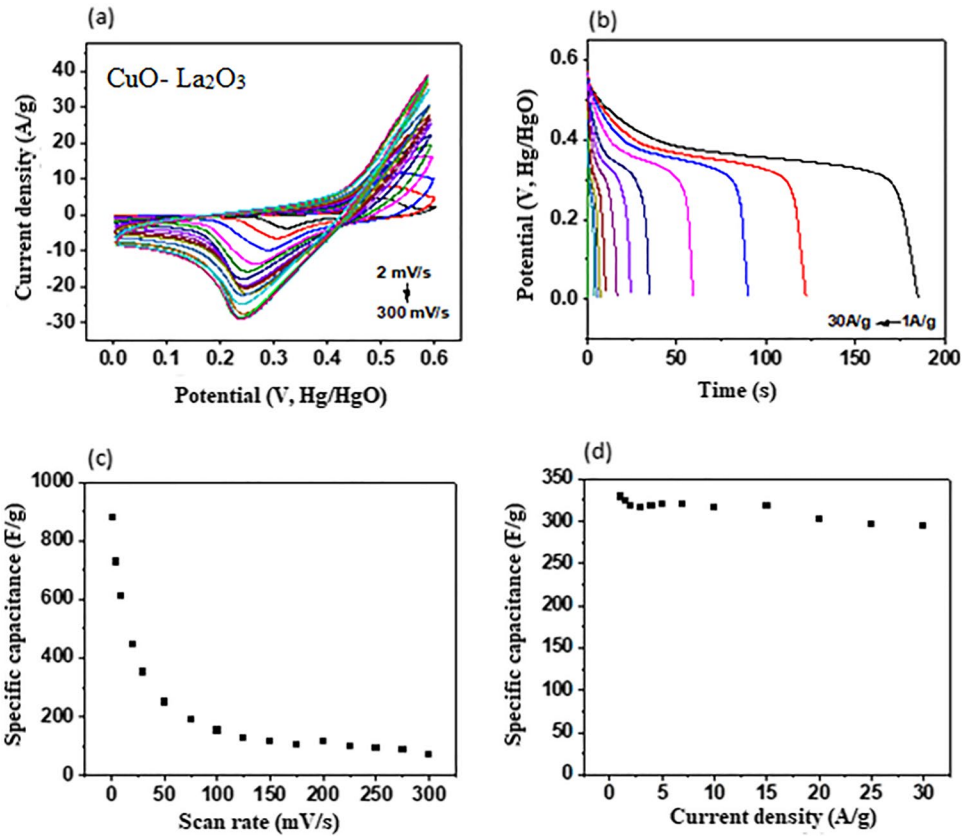

Fig. 7 Supercapacitor studies of CuO:La_2O_3-based electrode material: **a** CV analysis, **b** GCD analysis, **c** specific capacitance in terms of applied scan rates and **d** specific capacitance in terms of applied current densities

Table 1 Comparative study of the specific capacitance of AVL-CuO-ZrO_2 electrode with previously reported GCD studies

Electrode	Electrolyte	C_{sp} (F/g)	Current density Ag^{-1}	References
MoO_3–$NiMoO_4$	KOH	204	0.5	Shaheen et al. (2020)
Ag/Bi_2O_3	1 M KOH	82.1	5	Veeralakshami et al. (2020)
Carbon cloth nickel oxide–polyaniline (EC-NiP)	PANI	192.31	0.5	Razali et al. (2018)
Mo-doped ZnO nanoflakes	KOH	46.2	10	Ali et al. (2019)
CuO–La_2O_3	KOH	329	1	Present work

prepared electrode. Specific capacitance at all applied scan rates was measured using Eq. (3) and is presented in Fig. 7c:

$$\frac{\int IdV}{v.\Delta V.A}. \tag{3}$$

Here, Csp represents specific capacitance, v corresponds the scan rate, $\int$ IdV is the integral area of curve, ΔV depicts the possible window and A is the mass of active material (synthesized nanomaterial) deposited on the electrode. The CuO:La_2O_3-based electrode revealed the specific capacitance value of 879.6 F/g at the lowest scanning rate of 2 mV/s as given in Fig. 7c. This highest capacitance is better than numerous other reported CuO-based electrodes. Figure 7c also shows that the significant capacitance of 152 F/g was possessed even at high scan rate of 100 mV/s, indicating effective behavior of CuO:La_2O_3 toward supercapacitor.

The oxidation–reduction performance of the fabricated electrode was further studied by GCD, and obtained measurements endorsed the CV results as shown in Fig. 7b. Plateau kind and/or rectangular appearance as shown in Fig. 7b is depicting the pseudocapacitive nature of the fabricated electrode (Raveesha et al.2019; Dubal et al. 2013; Bu et al. 2017). The GCD also showed pattern which remained uniform at all current densities ranging from 0.5A/g to 30 A/g, hence illustrating the rate stability of electrode. The capacitance was also determined through GCD measurements using Eq. (4) and is presented in Fig. 7d:

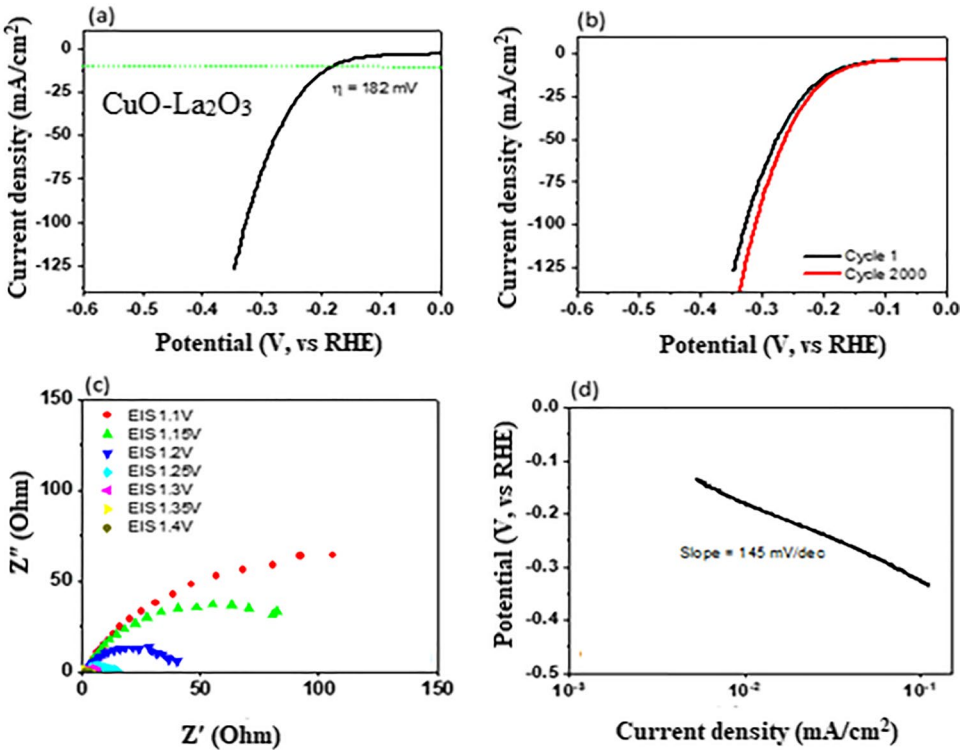

Fig. 8 HER studies of $CuO:La_2O_3$-based electrocatalyst: **a** polarization curve of fabricated electrode, **b** cyclic stability of $CuO:La_2O_3$-based electrode by LSV, **c** Nyquist plot **d** Tafel slope

Table 2 HER performance of $[CuO–La_2O_3]$ electro catalyst with reported metal oxide-based electrocatalysts

Electrocatalyst	Overpotential	Electrolyte	Tafel slope value (mV dec^{-1})	References
MnNi	360 mV	1 M KOH	_	Wu et al. (2017)
Amorphous MoSx	540 mV	1 M KOH	_	Liu et al. (2018)
NiO@NF	494 mV	1 M KOH	317	Wang et al. (2021)
Zn–Co–S nanosheets	413 mV	1 M KOH	139	Merki et al. (2011)
$CuO–La_2O_3$	182 mV	1 M KOH	145	Present research

$$C_{sp} = \frac{I \times \Delta t}{\Delta V \times m} \quad (4)$$

Here, I is for discharge current (A), Δt represents the discharging time (s), ΔV depicts the potential window (V), and m is for mass (g) of the material deposited on electrode. GCD data (Fig. 7d) indicates the specific capacitance value of 329 F/g at 1 A/g which is significantly better than number of reported electrodes as shown in Table 1.

The water splitting studies of fabricated electrodes was performed by using LSV and EIS. Linear sweep voltammetry (LSV) was employed to obtain the overpotential value of prepared electrode for HER measurements as shown in Fig. 8a. LSV measurements were taken at rate of 1 mV/s with ability of conversion to reversible hydrogen electrode (RHE) according to the Nernst Eq. (4) (Zahra et al. 2021):

$$ERHE = ESCE + 0.059pH + 0.1976. \quad (5)$$

The overpotential of 182 mV and the Tafel slope value of 145 mV/dec were obtained as shown in Fig. 8d. The comparison of obtained HER results with previously reported electrocatalyst is presented in Table 2 which depicts the excellent potential of fabricated electrocatalyst for hydrogen evolution reaction. Cyclic stability of the fabricated electrode was analyzed at various cyclic runs by using LSV (Fig. 8b). The results proved the excellent cyclic stability of the fabricated electrode till 2000th cycle at 10 mA/cm^2.

The conductance of the catalyst was investigated using electrochemical impedance spectroscopy as demonstrated

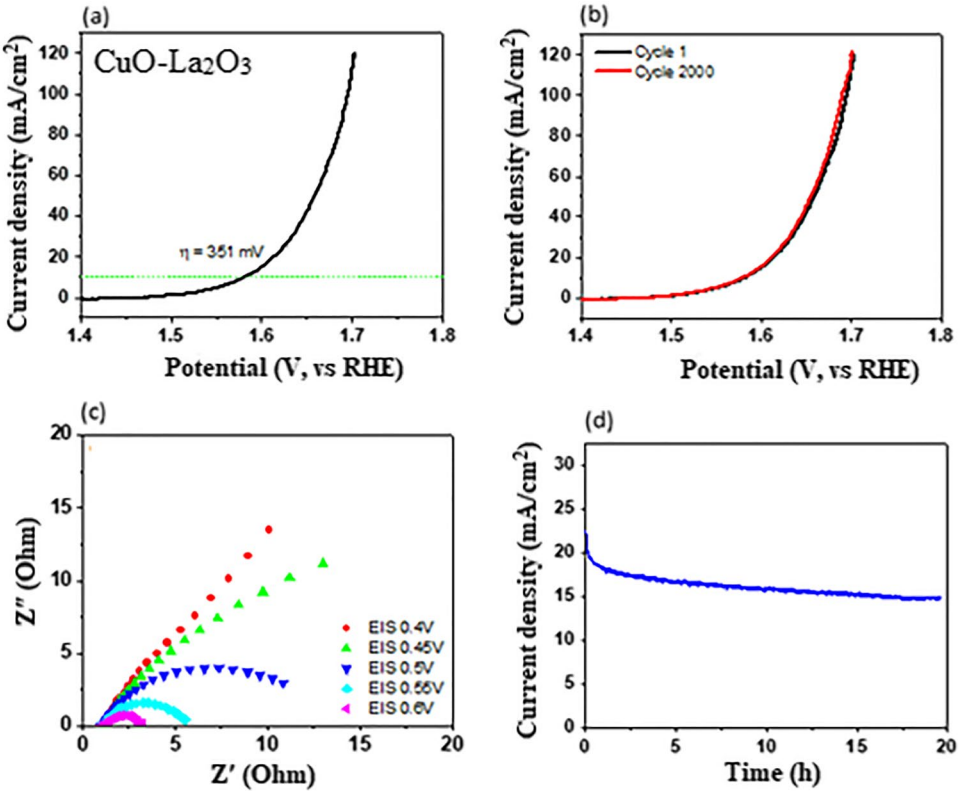

Fig. 9 OER studies of $CuO:La_2O_3$-based electrocatalyst: **a** polarization curve, **b** stability of $CuO:La_2O_3$ electrocatalyst by LSV, **c** Nyquist plot, **d** chronoamperometry test of $CuO:La_2O_3$ electrode

Table 3 OER performance of $[CuO–La_2O_3]$ electro catalyst with reported metal oxide-based electrocatalysts

Electrocatalyst	Overpotential	Electrolyte	Tafel slope value (mV/dec)	References
Er_2O_3-doped δ-Bi_2O_3	445 mV	1 M KOH	_	Azhar et al. (2023)
Co_3O_4/SWCNTS	550 mV	1 M KOH	104	Wu et al. (2012)
N-doped graphene NiCo2O4 hybrid paper	434 mV	_	_	Li et al. (2010)
$CuOLa_2O_3$	351	1 M KOH	_	Present work

in Fig. 8c. All EIS measurements were taken at alternating current (AC) of 10 mV amplitude and the frequency range of 0.05 Hz to 10 kHz. Overpotential (η) was calculated by using Eq. 5 (Doyle et al. 2013; Zhang et al. 2021):

$$\eta = \mathrm{ERHE} - 1.23V. \tag{6}$$

It was observed that the fabricated electrode demonstrated great conductive performance at even higher voltage with minimal value of charge transfer resistance.

Functionality of the prepared catalyst was investigated for OER measurements as well by using LSV and EIS, and the stability test was also carried out as given in Fig. 9. The obtained overpotential value of 351 mV is indicative of the excellent oxygen evolution performance of fabricated electrode which was further endorsed through comparative study with previous reported electrocatalyst as shown in Table 3. Exceptional durability of La_2O_3-doped CuO-based fabricated electrode was observed at several cyclic scans which depicts the prolonged life of catalyst. Likewise, the stability was additionally evaluated by chronoamperometry test which showed good response of material up to 20 h. The inverse conductivity trend was observed in the Nyquist plot (Fig. 9c) which was constructed using EIS data.

Accordingly, the fabricated $CuO:La_2O_3$-based electrode showed good electrochemical behavior for water splitting as well as for the supercapacitor. This can be attributed to the supreme effects due to the mixing of metal oxides which increase the oxygen vacancies, and hence, the competent oxidation–reduction behavior can be observed.

Conclusion

CuO:La_2O_3-based electrode was phyto-synthesized successfully using *Amaranthus viridis* L plant leaves. CuO:La_2O_3 was synthesized in different concentrations where the lowest crystal size of 18.2 nm was observed for 7.5% CuO:La_2O_3. The synthesized CuO:La_2O_3 nanomaterial exhibited efficient Faradic redox behavior with huge specific capacitance of 879.6 F/g. The water splitting further revealed effective results of HER and OER proposing the CuO:La_2O_3 as an potential electrocatalyst for water splitting. The phyto-genic strategy for synthesis of facile nanoelectrode materials is a preliminary phase toward development of sustainable energy storage as well as clean generation systems at the commercial scale.

Acknowledgements The authors acknowledge the Department of Environmental Sciences, Lab E-21, Fatima Jinnah Women University, Rawalpindi, and higher education commission of Pakistan. This work was supported by the Researchers Supporting Project Number (RSPD2023R667), King Saud University, Riyadh, Saudi Arabia.

Data availability Data would be available upon reasonable request to the corresponding author.

Declarations

Conflicts of interest The authors declare no conflict of interest.

References

Ali A, Ammar M, Ali M, Yahya Z, Javaid MY, ul Hassan Ahmed (2019) Mo-doped ZnO nanoflakes on Ni-foam for asymmetric supercapacitor applications. RSC Adv 9(47):27432–27438

Azhar S, Ahmad KS, Abrahams I, Lin W, Gupta RK, Mazhar M, Ali D (2021) Phyto-inspired Cu/Bi oxide-based nanocomposites: synthesis, characterization, and energy relevant investigation. RSC Adv 11(49):30510–30519

Azhar S, Ahmad KS, Abrahams I, Jaffri SB, Ingsel T, Gupta RK, Ali D (2023) Biomimetic [AV-Er2O3-doped δ-Bi2O3]-stacked nanoplates: an efficient electrocatalyst for OER/HER and electrode material for supercapacitor application. Ionics 27:1–6. https://doi.org/10.1007/s11581-023-05002-1

Bhagwan J, Hussain SK, Krishna BV, Yu JS (2020) β-NiS 3D microflower-based electrode for aqueous asymmetric supercapacitors, sustain. Energy Fuels 4:5550–5559

Bu IY, Huang R (2017) Fabrication of CuO-decorated reduced graphene oxide nanosheets for supercapacitor applications. Ceram Int 43:45–50

Chen TY, Vedhanarayanan B, Lin SY, Shao LD, Sofer Z, Lin JY, Lin TW (2020) Electrodeposited NiSe on a forest of carbon nanotubes as a free-standing electrode for hybrid supercapacitors and overall water splitting. J Cooloid Interface Sci 574:300–311

Dinesh M, Haldorai Y, Kumar RTR (2020) Mn–Ni binary metal oxide for high-performance supercapacitor and electro-catalyst for oxygen evolution reaction. Ceram Int 46:28006–28012

Doyle RL, Godwin IJ, Brandon MP, Lyons ME (2013) Redox and electrochemical water splitting catalytic properties of hydrated metal oxide modified electrodes. PCCP 15:13737–13783

Dubal DP, Gund GS, Lokhande CD, Holze R (2013) CuO cauliflowers for supercapacitor application: Novel potentiodynamic deposition. Mater Res Bull 48:923–928

Huang YY, Lin LY (2018) Synthesis of ternary metal oxides for battery-supercapacitor hybrid devices: influences of metal species on redox reaction and electrical conductivity. ACS Appl Energy Mater 1:2979–2990

Kumar A, Thomas A, Garg M, Perumal G, Grewal HS, Arora HS (2021) High performance CuO@ brass supercapacitor electrodes through surface activation. J Mater CheM 9:9327–9336

Li Y, Hasin P, Wu Y (2010) $NixCo_3-xO_4$ nanowire arrays for electrocatalytic oxygen evolution. Adv Mater 22(17):1926–1929. https://doi.org/10.1002/adma.200903896

Liu B, Qu S, Kou Y, Liu Z, Chen X, Wu Y, Zhong C (2018) In situ electrodeposition of cobalt sulfide nanosheet arrays on carbon cloth as a highly efficient bifunctional electrocatalyst for oxygen evolution and reduction reactions. ACS Appl Mater Interfaces 10(36):30433–30440

Mariadhas J, Panchu SJ, Swart HC, Rosaline DR, Murugadoss G, Govindarajan D, Kheawhom S, Inbanathan SS, Bokhari A, Chuah LF (2023) Microwave assisted green synthesis of Ag doped CuO NPs anchored on GO-sheets for high performance photocatalytic and antimicrobial applications. J Ind Eng Chem

Merki D, Fierro S, Vrubel H, Hu X (2011) Amorphous molybdenum sulfde flms as catalysts for electrochemical hydrogen production in water. Chem Sci 2:1262–1267. https://doi.org/10.1039/C1SC00117E

Mersian H, Alizadeh M, Hadi N (2018) Synthesis of zirconium doped copper oxide (CuO) nanoparticles by the Pechini route and investigation of their structural and antibacterial properties. Ceram Int 44(16):20399–20408

Nandi D, Mohan VB, Bhowmick AK, Bhattacharyya D (2020) Metal/metal oxide decorated graphene synthesis and application as supercapacitor: a review. J Mater Sci 55(15):6375–6400

Ramesh S, Khandelwal S, Rhee KY, Hui D (2018) Synergistic effect of reduced graphene oxide, CNT and metal oxides on cellulose matrix for supercapacitor applications. Compos B Eng 138:45–54

Raveesha HR, Sudhakar MS, Pratibha S, Ravikumara CR, Nagaswarupa HP, Dhananjaya N (2019) Costus Pictus leaf extract mediated biosynthesis of Fe and Mg doped CuO nanoparticles: structural, electrochemical and antibacterial analysis. Mater Res Exp 6(11):1150e5

Razali SA, Majid SR (2018) Electrochemical performance of binder-free NiO-PANI on etched carbon cloth as active electrode material for supercapacitor. Mater Des 5(153):24–35. https://doi.org/10.1016/j.matdes.2018.04.074

Sayyed SG, Mahadik MA, Shaikh AV, Jang JS, Pathan HM (2019) Nano-metal oxide based supercapacitor via electrochemical deposition. ES Energy Environ 3(7):25–44

Shaheen I, Ahmad KS, Zequine C, Gupta RK, Thomas AG, Malik MA (2020) Functionalization of MoO_3NiMoO_4 nanocomposite using organic template for energy storage application. J Energy Storage 29:101309. https://doi.org/10.1016/j.est.2020.101309

Shaheen I, Ahmad KS, Zequine C, Gupta RK, Thomas AG, Malik MA (2020) Green synthesis of ZnO–Co_3O_4 nanocomposite using facile foliar fuel and investigation of its electrochemical behaviour for supercapacitors. NJC 44:18281–18292

Shaheen I, Ahmad KS, Zequine C, Gupta RK, Thomas AG, Malik MA (2021) Modified sol-gel synthesis of Co_3O_4 nanoparticles using organic template for electrochemical energy storage. Energy 218:119502

Shinde SK, Yadav HM, Ghodake GS, Kadam AA, Kumbhar VS, Yang J, Kim DY (2019) Using chemical bath deposition to create nanosheet-like CuO electrodes for supercapacitor applications. Colloids Surf B 181:1004–1011

Tian Y, Liu Y, Wang WP, Zhang X, Peng W (2015) CuO nanoparticles on sulfur-doped graphene for nonenzymatic glucose sensing. Electrochim Acta 156:244–251

Tomboc GM, Kim J, Wang Y, Son Y, Li J, Kim JY, Lee K (2021) Hybrid layered double hydroxides as multifunctional nanomaterials for overall water splitting and supercapacitor applications. J Mater Chem a 9:4528–4557

Veerakumar P, Sangili A, Manavalan S, Thanasekaran P, Lin KC (2020) Research progress on porous carbon supported metal/metal oxide nanomaterials for supercapacitor electrode applications. Ind Eng Chem Res 59:6347–6374

Veeralakshmi S, Kalaiselvam S, Murugan R, Pandurangan P, Nehru S, Sakthinathan S, Chiu TW (2020) An approach to develop high performance supercapacitor using Bi_2O_3 based binary and ternary nanocomposites. J Mater Sci: Mater Electron 31:22417–22426. https://doi.org/10.1007/s10854-020-047433

Wang S, Hu J, Jiang L, Li X, Cao J, Wang Q, Lu Y (2019) High–performance 3D CuO/Cu flowers supercapacitor electrodes by femtosecond laser enhanced electrochemical anodization. Electrochim Acta 293:273–282

Wang J, Xu F, Jin H, Chen Y, Wang Y (2021) Non-noble metalbased carbon composites in hydrogen evolution reaction: fundamentals to applications. Adv Mat 14:1605838

Wei G, He J, Zhang W, Zhao X, Qiu S, An C (2018) Rational design of Co (II) dominant and oxygen vacancy defective $CuCo_2O_4$@CQDs hollow spheres for enhanced overall water splitting and supercapacitor performance. Inorg Chem 57:7380–7389

Wu J, Xue Y, Yan X, Yan W, Cheng Q, Xie Y (2012) Co3O4 nanocrystals on single-walled carbon nanotubes as a highly efcient oxygen-evolving catalyst. Nano Res 5:521–530. https://doi.org/10.1007/s12274-012-0237-y

Wu X, Han X, Ma X, Zhang W, Deng Y, Zhong C, Hu W (2017) Morphology-controllable synthesis of Zn–Co-mixed sulfde nanostructures on carbon fber paper toward efcient rechargeable zinc–air batteries and water electrolysis. ACS Appl Mat Interf 9:12574–12583. https://doi.org/10.1021/acsami.6b16602

Yan S, Abhilash KP, Tang L, Yang M, Ma Y, Xia Q, Xia H (2019) Research advances of amorphous metal oxides in electrochemical energy storage and conversion. Small 15:1804371

Yumak T, Bragg D, Sabolsky EM (2019) Effect of synthesis methods on the surface and electrochemical characteristics of metal oxide/activated carbon composites for supercapacitor applications. Appl Surf Sci 469:983–993

Zahra T, Ahmad KS, Zequine C, Gupta R, Thomas AG, Malik MA (2020) Evaluation of electrochemical properties of organic template assisted PdO incorporated NiO for H_2/O_2 evolution. Microchem J 158:105282

Zahra T, Ahmad KS, Zequine C, Gupta RK, Thomas AG, Malik MA, Ali D (2021) Electro-catalyst [ZrO2/ZnO/PdO]-NPs green functionalization: fabrication, characterization and water splitting potential assessment. Int J Hydrog Energy 46:19347–19362

Zequine C, Bhoyate S, Wang F, Li X, Siam K, Kahol PK, Gupta RK (2019) Effect of solvent for tailoring the nanomorphology of multinary CuCo2S4 for overall water splitting and energy storage. J Alloy Compd 784:1–7

Zhang P, Liu X, He H, Peng Y, Wu Y (2020) Engineering RuO_2 on $CuCo_2O_4$/CuO nanoneedles as multifunctional electrodes for the hybrid supercapacitors and water oxidation catalysis. J Alloys Compds 832:154962

Zhang L, Zhao H, Xu S, Liu Q, Li T, Luo Y, Sun X (2021) Recent advances in 1D electrospun nanocatalysts for electrochemical water splitting. Structures 2:2000048

Zheng JH, Zhang RM, Yu PF, Wang XG (2019) Binary transition metal oxides (BTMO)(Co-Zn, Co-Cu) synthesis and high supercapacitor performance. J Alloys Compds 772:359–365

Authors and Affiliations

Sundus Azhar[1] · Khuram Shahzad Ahmad[1] · Isaac Abrahams[2] · Tenzin Ingsel[3] · Ram K. Gupta[3] · Adel El-marghany[4]

✉ Khuram Shahzad Ahmad
chemist.phd33@yahoo.com; dr.k.s.ahmad@fjwu.edu.pk

[1] Materials and Environmental chemistry Lab, Lab E-21, Department of Environmental Sciences, Fatima Jinnah Women University, Rawalpindi, Pakistan

[2] School of Biological and Chemical Sciences, Queen Mary University of London, London, UK

[3] Department of Chemistry, Pittsburg State University, Pittsburg, KS 66762, USA

[4] Department of Chemistry, College of Science, King Saud University, P.O. Box 2455, 11451 Riyadh, Saudi Arabia